Measurement of the properites of cosmic rays with the LOFAR radio telescope

Jörg R. Hörandel[1,2,*] A. Bonardi[1], S. Buitink[1,3], A. Corstanje[1], H. Falcke[1,2,4,5], B. Hare[6], P. Mitra[3], K. Mulrey[3], A. Nelles[1,2,8], J.P. Rachen[1], L. Rossetto[1], P. Schellart[1,9], O. Scholten[6,7], S. ter Veen[4], S. Thoudam[1,10], T.N.G. Trinh[6], and T. Winchen[3]

[1] *Department of Astrophysics, IMAPP, Radboud University Nijmegen, P.O. Box 9010, 6500 GL Nijmegen, The Netherlands*

[2] *NIKHEF, Science Park Amsterdam, Amsterdam 1098 XG, The Netherlands*

[3] *Astrophysical Institute, Vrije Universiteit Brussel, Pleinlaan 2, Brussels 1050, Belgium*

[4] *ASTRON, Postbus 2, Dwingeloo 7990 AA, The Netherlands*

[5] *Max-Planck-Institut für Radio Astronomie, Bonn, Germany*

[6] *KVI-CART, Groningen University, P.O. Box 72, Groningen 9700 AB, The Netherlands*

[7] *Interuniversity Institute for High Energies, Vrije Universiteit Brussel, Pleinlaan 2, 1050 Brussels, Belgium*

[8] *now at: Department of Physics and Astronomy, University of California Irvine, Irvine, CA 92697-4575, USA*

[9] *now at: Department of Astrophysical Sciences, Princeton University, Princeton, NJ 08544, USA*

[10] *now at: Department of Physics and Electrical Engineering Linneuniversitetet, 35195 Växjö, Sweden*

[*] *http://particle.astro.ru.nl*

High-energy cosmic rays, impinging on the atmosphere of the Earth initiate cascades of secondary particles, the extensive air showers. The electrons and positrons in the air shower emit electromagnetic radiation. This emission is detected with the LOFAR radio telescope in the frequency range from 10 to 240 MHz. The data are used to determine the properties of the incoming cosmic rays. The radio technique is now routinely used to measure the arrival direction, the energy, and the particle type (atomic mass) of cosmic rays in the energy range from 10^{17} to 10^{18} eV. This energy region is of particular astrophysical interest, since in this regime a transition from a Galactic to an extra-galactic origin of cosmic rays is expected. For illustration, the LOFAR results are used to set constraints on models to describe the origin of high-energy cosmic rays.

I. INTRODUCTION

Cosmic rays (ionized atomic nuclei) impinge on the Earth with (kinetic) energies covering a wide range from MeV energies up to beyond 10^{20} eV. At energies below $\sim$ 100 MeV they are accelerated in energetic outbursts of the Sun. At higher energies, the are assumed to originate in our Milky Way, being accelerated in Supernova remnants, e.g. [1, 2]. At energies exceeding 10^{18} eV it becomes increasinlgy difficult to magnetically bind the particles to our Galaxy. Thus, particles with energies above $\sim 10^{18}$ eV are usually considered to be of extra-galactic origin. A transition from a Galactic to an extra-galactic origin of cosmic rays is expected at energies around 10^{17} to 10^{18} eV [3, 4].

Understanding the origin of cosmic rays in the transition region ($10^{17} - 10^{18}$ eV) necessitates a precise measurement of the properties of cosmic rays, namely their arrival direction (on the sky), their (kinetic) energy, and their particle type (atomic mass A). The radio detection of air showers provides a new tool for such measurements.

The flux of cosmic rays is steeply falling, approximately following a power law $\propto E^{-3}$. In our region of interest, cosmic rays are only measured indirectly, using large ground-based detector installations. High-energy cosmic rays impinging on the atmosphere, initiate cascades of secondary particles, the extensive air showers. The challenge of the indirect measurements is to derive the properties of the incoming cosmic rays from air-shower observations. Most challenging is the measurement of the particle type, since the sensitivity of air shower measurements is only proportional to $\ln A$. Intrinsic shower fluctuations allow to divide the measured cosmic rays in up to five mass groups for the best experiments [5].

The radio measurement of air showers is briefly sketched in Sect. II. The method is used to determine the properties of cosmic rays as outlined in Sect. III. One of the key results obtained is the mass composition of cosmic rays in the transition region. Impli-

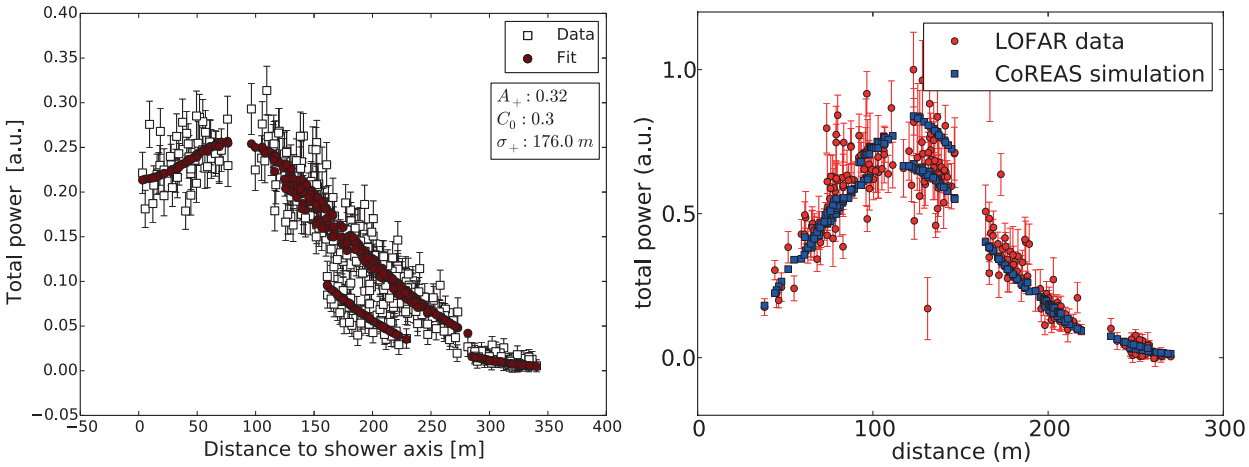

FIG. 1: Air showers measured with LOFAR [6, 7]. The total power as a function of the distance to the shower axis in the frequency range $30 - 80$ MHz (left) and $110 - 190$ MHz (right).

cations on our understanding of the origin of cosmic rays will be discussed.

II. RADIO DETECTION OF AIR SHOWERS

Many secondary particles in extensive air showers are electrons and positrons. They emit radiation with frequencies of tens of MHz mainly due to interaction with the magnetic field of the Earth. Radio detection of air showers is suitable to measure the properties of cosmic rays with nearly 100% duty cycle [8, 9].

A. LOFAR

The LOFAR radio telescope [10, 11] is one of the leading installations for the radio measurements of air showers. LOFAR is a digital radio telescope. Its antennas are spread over several European countries and are used together for interferometric radio observations in the frequency range of $10 - 240$ MHz. The density of antennas increases towards the center of LOFAR, which is located in the Netherlands. Here, about 2400 antennas are clustered on an area of roughly 10 km^2 with increasing antenna density towards the center. This high density of antennas makes LOFAR the perfect tool to study features of the radio emission created by extensive air showers. The radio antennas have been calibrated with in-situ measurements, using a reference source and Galactic emission [12].

Air shower measurements are conducted based on a trigger received from an array of scintillators (LORA) [13, 14], which results in a read-out of the ring buffers that store the raw voltage traces per antenna for up to 5 s. LOFAR comprises two types of antennas. While air showers have also been measured in the high frequency band ($110 - 240$ MHz), most air showers are measured with the low-band antennas (LBA), which cover the frequency range from $10 - 90$ MHz. The LBAs are arranged in compact clusters of 96 antennas, called stations. Of every station either the inner group or the outer ring of antennas (48 antennas each) can be used for cosmic-ray measurements at a given time.

B. Radio emission

In the last years the radio technique has been established as a precise method to measure the mass composition of cosmic rays. In addition to LOFAR, radio emission from extensive air showers has also been measured in detail by the pioneering experiments LOPES [15, 16] and CODALEMA [17–19] and on larger scales by Tunka-REX [20] and the Auger Engineering Radio Array – AERA at the Pierre Auger Observatory [21, 22].

The LOFAR measurements together with the predictions of the CoREAS [23] simulation package result in a complete understanding of the emission mechanisms. With LOFAR the properties of the radio emission have been measured with high accuracy [24–26] in the frequency range $30 - 80$ MHz, which allows us to establish key features of the radio emission.

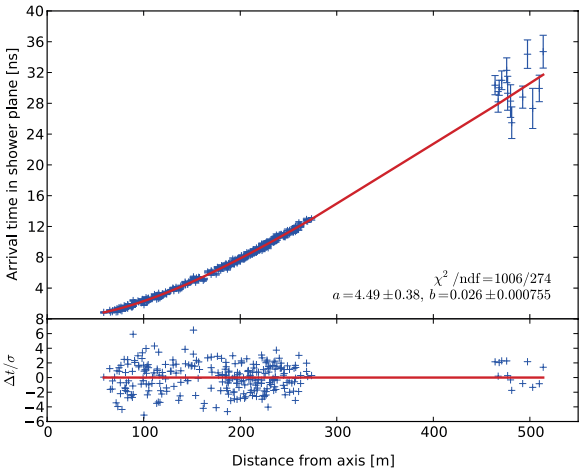

FIG. 2: Arrival time of the signals as a function of the distance to the shower axis [28]. The lower graph illustrates the arrival time differences with respect to a fit (hyperboloid).

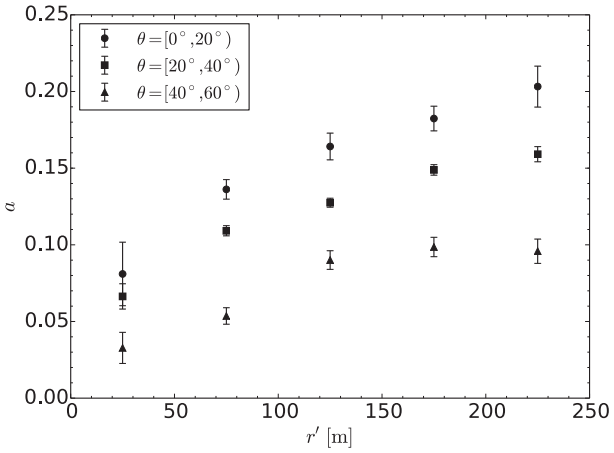

FIG. 3: Radio emission processes in the atmosphere [32]. The ratio between Askaryan effect and geomagnetic emission is plotted as a function of the distance to the shower axis for showers with different zenith angles, as indicated, and measured by LOFAR.

C. Lateral distribution function of the radio signals

The footprint of the radio emission recorded at ground level is not rotationally symmetric, such as e.g. the particle content of a shower [6, 27]. Radio emission is generated through interactions with the Earth magnetic field, which yield a bean-shaped footprint on the ground. The measured power is plotted as a function of the distance to the shower axis in Fig. 1 in the frequency bands 30−80 MHz (left) and 110−190 MHz (right). For example at a distance of 200 m from the shower axis in the left figure, ambiguities are visible in this one-dimensional projection: the recorded signal strength is a function of the azimuth angle, which results in the visible structure. The power density of the radio emission can be parameterized by an analytical expression: a two-dimensional Gaussian function is used to describe the approximately exponential fall-off at large distances form the shower axis. A second (smaller) two-dimensional Gaussian function is subtracted from the first one to describe the ring structure of the signal close to the shower axis. To reproduce the observed bean shape, the centres of both Gaussian functions are slightly offset.

D. Shape of the shower front

The precise shape of the radio wave front is a long-standing issue [28, 29]. In the literature different scenarios have been discussed: a spherical shape or a conical shape. The LOFAR findings clearly indicate that a hyperboloid is the best way to describe the shape of the measured wave front, confirming first hints from LOPES [30, 31]. A hyperboloid asymptotically reaches a conical shape at large distances from the shower axis and can be approximated as a sphere close to the shower axis. A measured wave front of a shower registered with LOFAR is shown in Fig. 2. The time difference relative to a plane is plotted as a function of a distance to the shower axis. The line indicates a fit of a hyperboloid to the measured data. The lower part of the graph shows the time differences of the individual antennas with respect to the fit function.

E. Polarization of the radio signal

The radio emission in extensive air showers originates from different processes [32, 33]. The dominant mechanism is of geomagnetic origin [16, 34–38]. Electrons and positrons in the shower are accelerated in opposite directions by the Lorentz force exerted by the magnetic field of the Earth. The generated radio emission is linearly polarized in the direction of the Lorentz force ($v \times B$), where v is the propagation velocity vector of the shower (parallel to the shower axis) and B represents the direction and strength of the Earth magnetic field. A secondary contribution to the radio emission results from the excess of electrons at the front of the shower (Askaryan effect) [39]. This excess is built up from electrons that are knocked out of atmospheric molecules by interactions with shower particles and by a net depletion of positrons due to annihilation. This charge excess contribution is radially polarized, pointing towards the shower axis. The resulting emission measured at the ground is the sum of both components. Interference between these com-

ponents may be constructive or destructive, depending on the position of the observer/antenna relative to the shower. The emission is strongly beamed in the forward direction due to the relativistic velocities of the particles. Additionally, the emission propagates through the atmosphere, which has a non-unity index of refraction that changes with height. This gives rise to relativistic time-compression effects, most prominently resulting in a ring of amplified emission around the Čerenkov angle, see Fig. 1, right. By precisely measuring the polarization direction of the electric field in each LOFAR antenna we determine the relative contribution of the main emission processes, thus clarifying the emission processes in air showers. The parameter a gives the ratio of the charge excess contribution to the geomagnetic radiation. This ratio is depicted in Fig. 3 as a function of the distance to the shower axis. Measurements for showers with different zenith angles are shown. The figure illustrates that the contribution through the Askaryan effect increases with increasing distance to the shower axis and it is more pronounced for vertical showers (with small zenith angle). Corresponding investigations at AERA yield an average value $a = 14\% \pm 2\%$ [40].

F. First quantitative measurements in the frequency range 120-240 MHz

Radio emission from extensive air showers has also been recorded with the high-band antennas in the 200 MHz frequency domain [7]. The measured power is depicted in Fig. 1, right as a function of the distance to the shower axis. A clear maximum is visible at distances around 120 m, indicating a clear (Čerenkov) ring structure. Such rings are predicted from theory: relativistic time compression effects lead to a ring of amplified emission, which starts to dominate the emission pattern for frequencies above $\sim$ 100 MHz. The LOFAR data clearly confirm the importance to include the index of refraction of air as a function of height into calculations of the radio emission (see also [41]).

G. Probing atmospheric electric fields during thunderstorms

Radio detection of air showers is also used for auxiliary science, such as the measurements of electric fields in the atmosphere during thunderstorms [42, 43]. The footprint of the radio emission from an air shower, which developed during a thunderstorm is shown in Fig. 4. The intensity and polarization patterns of such air showers are radically different from those measured during fair-weather conditions. The figure illustrates the polarization as measured with individual LOFAR antennas (arrows) in the shower plane. LOFAR antennas are grouped into circular stations, of which seven are depicted. An arrow labelled normal indicates the expected polarization direction for fair weather conditions. The position of the shower axis, orthogonal to the shower plane, is indicated by the intersection of the dashed lines. With the use of a simple two-layer model for the atmospheric electric field, these patterns can be well reproduced by state-of-the-art simulation codes. This in turn provides a novel way to study atmospheric electric fields.

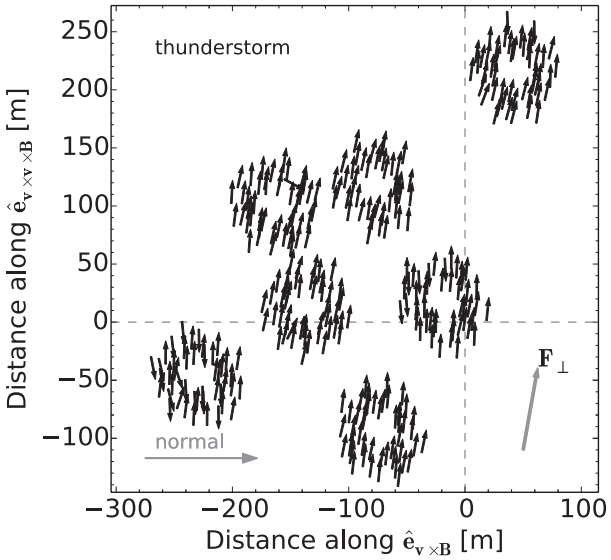

FIG. 4: Footprint of the radio emission of an air shower, which developed during a thunderstorm [42].

These measurements, together with findings from other groups [38, 40, 44–46] help to understand the emission processes in the atmosphere and to quantify the contributions of the two mechanisms, being responsible for the radio emission of air showers – namely the geomagnetic effect (i.e. charge separation in the geomagnetic field) and the Askaryan effect (charge excess in the shower front). This allows to reconstruct the properties of the incoming cosmic rays from the radio measurements as explained in the following section.

III. PROPERTIES OF COSMIC RAYS

Ultimate goal is to derive the properties of the incoming cosmic ray from the radio measurements, namely their arrival direction (via the precise measurement of the arrival time of the radio waves in the shower front, as described above), their energy, and their particle type/atomic mass. The parame-

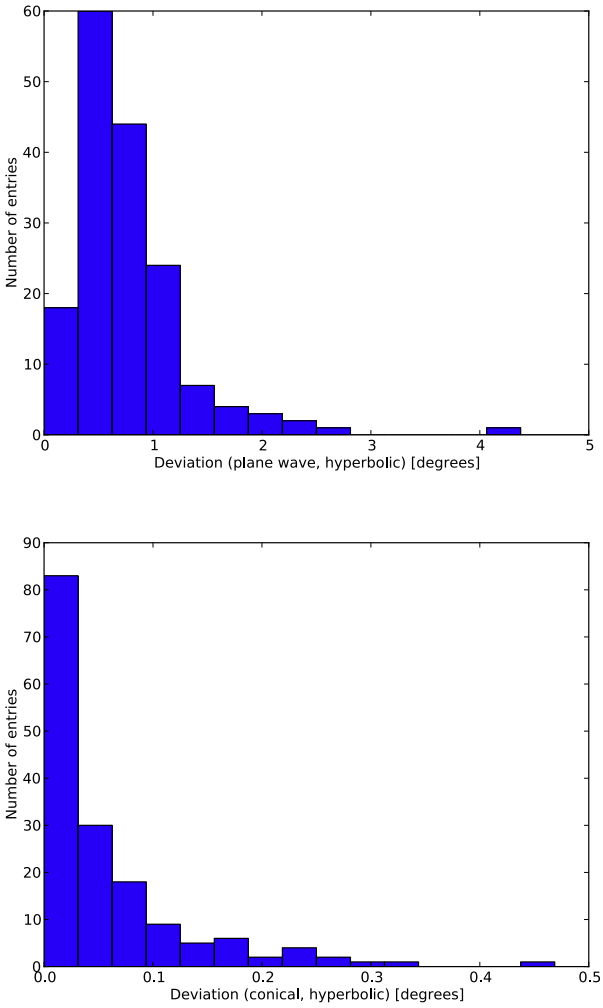

FIG. 5: Angular difference between reconstructed shower axis direction for three wavefront shape assumptions. Assuming a planar wavefront shape typically introduces an error in the direction of up to $\sim 0.1^\circ$, when the shape is in fact hyperbolic (top plot). The differences in reconstructed direction between a conical and hyperbolic wavefront shape are approximately a factor of ten smaller (bottom plot) [28].

ters of the function to model the intensity pattern of the radiation on the ground (as described above) are sensitive to the properties of the shower-inducing cosmic rays. The integral of the measured power density is proportional to the shower energy. The width of the measured footprint is proportional to the distance from the antennas to the position of the shower maximum, which in turn can be used to determine $X_{\max}$ and the mass of the cosmic ray.

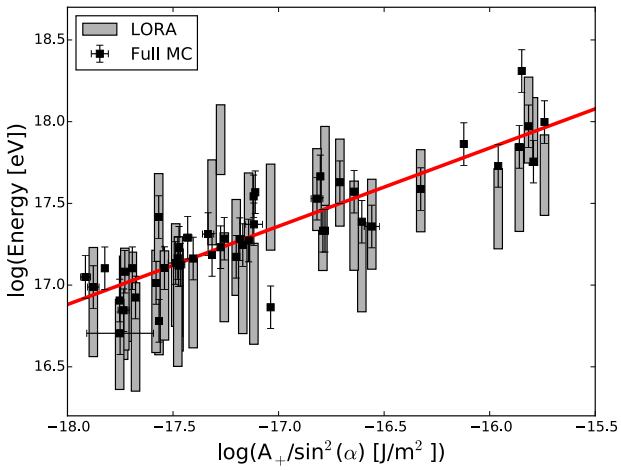

FIG. 6: The energy as obtained from the particle detectors LORA (grey bands) and the energy from the full Monte-Carlo approach (black squares) are shown as a function of the fit parameter A_+, i.e. the normalization of the two-dimensional Gaussian function. Air showers with no grey bands are more horizontal than 45°. The straight line shows the best fit to the full Monte-Carlo energies. Updated from [6].

A. Direction

The excellent time resolution of LOFAR with ns accuracy allows to measure the shape of the shower front [28]. In order to estimate the accuracy of the measurement of the arrival direction of the shower, the same measured air showers have been reconstructed with different assumptions (plane, sphere, hyperboloid) as depicted in Fig. 5. These investigations indicate an uncertainty for the direction reconstruction of the order of 0.1°to 0.5°.

B. Energy

The recording of radio signals in the frequency range of interest ($30 - 80$ MHz) provides an excellent calorimetric measure of the energy contained in the electromagnetic component of the air shower and, thus, provides a good measure of the energy of the shower-inducing particle. The integral over the measured energy fluence distribution on the ground is proportional to the energy of the incoming cosmic ray. This is illustrated in Fig. 6, the shower energy is obtained in two ways: measured with the LORA scintillator array and obtained from Monte-Carlo simulations. The results of both methods are plotted against the overall normalization parameter A_+ of the two-dimensional Gaussian function, for details see [6]. A resolution around 30% for the cosmic-ray energy is obtained with LOFAR [47]. Similar investigations at the Pierre Auger Observatory indicate that a resolu-

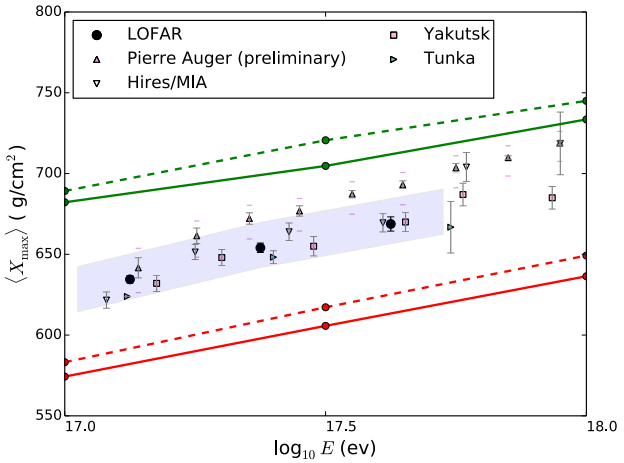

FIG. 7: Average depth of the shwoer maximum $X_{\rm max}$ as a function of cosmic-ray energy [50]. The LOFAR radio results are compared to optical measurements. For details and references see [50]. The lines represent predictions for protons (green) and iron nuclei (red) for the hadronic interaction models QGSJETII.04 (solid) and EPOS-LHC (dashed).

tion around 25% is possible for high-quality showers [48, 49].

C. Particle type

The good agreement between the measurements and the predictions of the CoREAS code is essential to identify the type of incoming cosmic ray. This is inferred from the (atmospheric) depth of the shower maximum $X_{\rm max}$, one of the standard measures to estimate $\ln A$. Radio measurements of air showers are used to derive $X_{\rm max}$ [52–54].

To measure $X_{\rm max}$ with LOFAR [47, 50] we analyse simultaneously measurements of the radio emission and the particle detectors. The arrival direction and energy of each cosmic ray are determined first. Then, simulations for primary protons and iron nuclei are conducted for each measured shower with its corresponding direction and energy. Due to the intrinsic shower fluctuations is it sufficient to simulate only protons and iron nuclei to cover the parameter space in $X_{\rm max}$. The predictions for the signals in the particle detectors and the radio antennas are compared on a statistical basis to the measured values. This method is used to determine $X_{\rm max}$ with an accuracy of better than ~ 20 g/cm^2 with the dense LOFAR core, thus, reaching the state of the art – the uncertainty of the Pierre Auger Observatory fluorescence detector. The $X_{\rm max}$ values obtained are depicted as a function of energy in Fig. 7 together with other measurements. The latter apply different techniques, namely measuring Čerenkov and fluorescence light from the air showers. The figure illustrates the good agreement between the radio measurements and the established optical methods.

An important systematic effect is the refractive index of the air n and its dependence on atmospheric conditions, such as pressure, temperature, and humidity. Recent investigations show that the refractivity $N = 10^6(n-1)$ can have relative variations of the order of 10% depending on atmospheric parameters, typical variations are of the order of 4%. They result in a systematic uncertainty of the depth of the shower maximumof a few $(3.5-11)$ g/cm^2 [41].

The measured values for the depth of the shower maximum $X_{\rm max}$ are converted to the mean logarithmic mass of cosmic rays

$$\langle \ln A \rangle = \left(\frac{X_{\rm max} - X^{\rm p}_{\rm max}}{X^{\rm Fe}_{\rm max} - X^{\rm p}_{\rm max}} \right) \times \ln A_{\rm Fe}.$$

This necessiates predictions for the depth of the shower maximum for impinging protons and iron nuclei, $X^{\rm p}_{\rm max}$ and $X^{\rm Fe}_{\rm max}$, respectively. These are illustrated as lines in Fig. 7: protons (green) and iron nuclei (red). The resulting mean mass is depicted in Fig. 8 (left) as a function of energy for the LOFAR results together with the world data set [51]. Two hadronic interaction models are used (EPOS-LHC and QGSJETII.04, dashed and solid lines in Fig. 7, respectively) to interpret the data. Both interaction models are tuned to LHC data but uncertainties remain, when extrapolating to the cosmic-ray parameter space.

D. Origin of cosmic rays

To understand the implications of the LOFAR measurements and the available world data set from direct and indirect measurements a model has been developed to consistently describe the observed energy spectrum and mass composition of cosmic rays with energies up to about 10^{18} eV [51]. We assume that the bulk of Galactic cosmic rays is accelerated by strong Supernova remnant shock waves [55]. Our study shows that a single Galactic component with rigidity-dependent energy cut-offs in the individual spectra of different elements cannot explain the observed all-particle spectrum at energies exceeding $\sim 2 \cdot 10^{16}$ eV. Similar findings have already been obtained earlier [56]. We discuss two approaches for a second component of Galactic cosmic rays: re-acceleration at a Galactic wind termination shock and Supernova explosions of Wolf-Rayet stars. The latter scenario can explain almost all observed features in the all-particle spectrum and the mass composition of cosmic rays up to $\sim 10^{18}$ eV, when combined with a canonical extra-galactic spectrum as expected from strong radio galaxies or a source population with similar cosmological evolution. The resulting spectrum is shown in

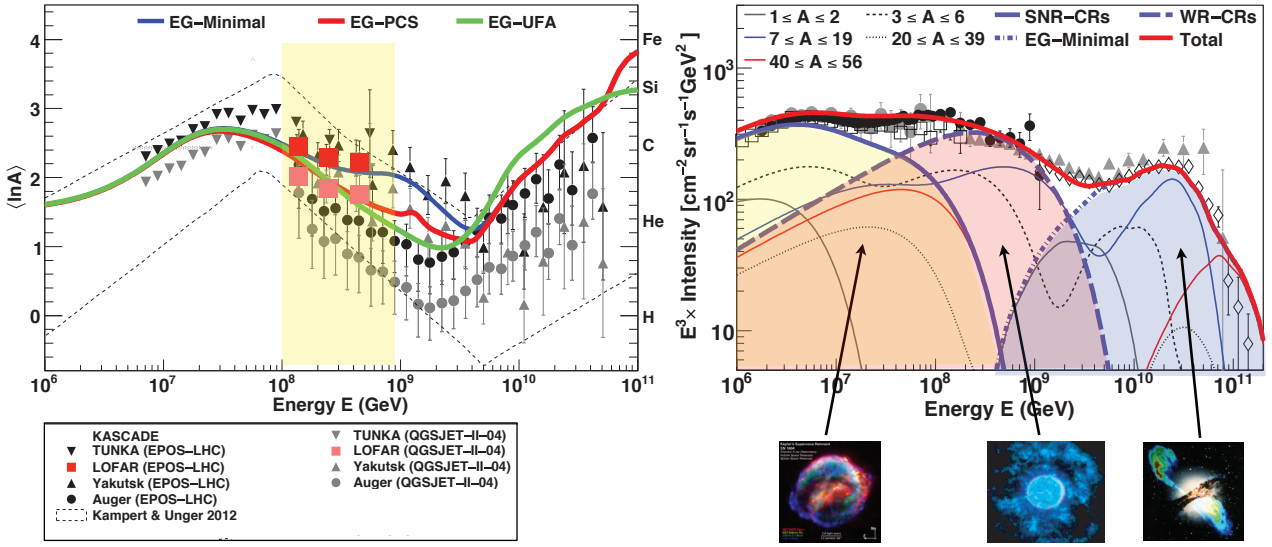

FIG. 8: Left: Mean logarithmic mass of cosmic rays as a function of energy, for details, see [51]. Right: Three-component model of the origin of cosmic rays according to [51]: 'regular' supernovae, Wolf Rayet component, and an extra-galactic component.

Fig. 8 (right). In this two-component Galactic cosmic-ray model, the 'knee' at $\sim 4 \cdot 10^{15}$ eV and the 'second knee' at $\sim 4 \cdot 10^{17}$ eV in the all-particle spectrum are due to the fall-offs of the first and second Galactic cosmic-ray components, respectively.

IV. CONCLUSIONS

The radio detection of extensive air showers enables us to measure the properties of cosmic rays above energies exceeding 10^{17} eV with high precision of $\sim 0.1^\circ - 0.5^\circ$for the arrival direction, $\sim 30\%$ for the energy, and to better than ~ 20 g/cm^2 for the depth of the shower maximum $X_{\max}$.

To illustrate the potential of the LOFAR radio measurements we developed a model to consistently describe the observed energy spectrum and mass composition of cosmic rays from GeV energies up to 10^{20} eV. We adopt a three component model: 'regular' cosmic rays being accelerated in Supernova remnants up to $\sim 10^{17}$ eV, a second Galactic component, dominating the all-particle flux between $\sim 10^{17}$ and $\sim 10^{18}$ eV from cosmic rays being accelerated by exploding Wolf-Rayet stars, yielding a strong contribution of He and CNO elements, and, finally, an extra-galactic contribution at energies above $\sim 10^{18}$ eV.

V. ACKNOWLEDGEMENTS

JRH is grateful to the organizers of the ECRS for their kind invitation.

[1] F. Aharonian, et al., Astron. & Astroph. 449 (2006) 223.
[2] H. Völk, E. Berezhko, Astron. & Astroph. 451 (2006) 981.
[3] J. Blümer, R. Engel, J. Hörandel, Prog. Part. Nucl. Phys. 63 (2009) 293.
[4] M. Nagano, A. Watson, Rev. Mod. Phys. 72 (2000) 689.
[5] J. Hörandel, Nucl. Instr. & Meth. A 588 (2008) 181.
[6] A. Nelles, et al., JCAP 1505 (05) (2015) 018.
[7] A. Nelles, et al., Astropart.Phys. 65 (2014) 11–21.
[8] T. Huege, Phys. Rept. 620 (2016) 1–52.
[9] F. G. Schröder, Prog. Part. Nucl. Phys. 93 (2017) 1–68.
[10] M. van Haarlem, et al., Astronomy & Astrophysics 556 (2013) A2.
[11] P. Schellart, et al., Astron.Astrophys. 560 (2013) A98.
[12] A. Nelles, et al., JINST 10 (11) (2015) P11005.
[13] S. Thoudam, et al., Nucl.Instrum.Meth. A767 (2014) 339–346.
[14] S. Thoudam, et al., Astropart. Phys. 73 (2016) 34–43.
[15] A. Horneffer, et al., Proc. of the SPIE 5500 (2004) 129.
[16] H. Falcke, et al., Nature 435 (2005) 313.
[17] D. Ardouin, et al., Nucl. Instr. & Meth. A 555 (2005) 148.
[18] O. Ravel, et al., Nucl. Instrum. Meth. A518 (2004) 213–215.

[19] C. Riviere, et al., arXiv:0906.2720 (2009).
[20] F. G. Schröder, et al., JPS Conf. Proc. 9 (2016) 010008.
[21] P. Abreu, et al., Nucl.Instrum.Meth. A635 (2011) 92–102.
[22] P. Abreu, et al., JINST 7 (2012) P10011.
[23] T. Huege, M. Ludwig, C. W. James, AIP Conf. Proc. 1535 (2013) 128.
[24] J. Hörandel, et al., Proceedings of the 33rd International Cosmic Ray Conference, Rio de Janeiro (2013) 865.
[25] J. Hörandel, et al., Proceedings of the 34th International Cosmic Ray Conference, Den Haag (2015) PoS(ICRC2015)033.
[26] J. R. Hörandel, JPS Conf. Proc. 9 (2016) 010004.
[27] A. Nelles, et al., Astropart.Phys. 60 (2015) 13–24.
[28] A. Corstanje, et al., Astropart.Phys. 61 (2015) 22–31.
[29] A. Corstanje, et al., Astron. Astrophys. 590 (2016) A41.
[30] F. G. Schröder, et al. LOPES collaboration, Proceedings of the International Cosmic Ray Conference, Vol. 3 (2011), 64.
[31] W. Apel, et al., JCAP 1409 (09) (2014) 025.
[32] P. Schellart, et al., JCAP 1410 (10) (2014) 014.
[33] O. Scholten, et al., Phys. Rev. D94 (10) (2016) 103010.
[34] F. Kahn, I. Lerche, Royal Society of London Proceedings Series A 289 (1966) 206.
[35] H. Allan, Progress in Elementary Particles and Cosmic Ray Physics, J.G. Wilson and S.G. Wouthuysen eds., North Holland, 1971, p. 169.
[36] H. Falcke, P. Gorham, Astropart. Phys. 19 (2003) 477–494.
[37] T. Huege, et al., Nucl. Instrum. Meth. A662 (2012) S72–S79.
[38] D. Ardouin, et al., Astropart. Phys. 31 (2009) 192–200.
[39] G. Askaryan, Journal of the Physical Society of Japan Supplement 17 (1962) C257.
[40] A. Aab, et al., Phys.Rev. D89 (5) (2014) 052002.
[41] A. Corstanje, et al., Astropart. Phys. 89 (2017) 23–29.
[42] P. Schellart, et al., Phys.Rev.Lett. 114 (16) (2015) 165001.
[43] T. N. G. Trinh, et al., Phys. Rev. D93 (2) (2016) 023003.
[44] B. Revenu, et al., arXiv:0906.2832 (2009).
[45] V. Marin, in: Proceedings, 32nd International Cosmic Ray Conference (ICRC 2011), Vol. 1, 2011, pp. 291–294.
[46] A. Bellétoile, et al., Astropart.Phys. 69 (2015) 50–60.
[47] S. Buitink, et al., Phys.Rev. D90 (8) (2014) 082003.
[48] A. Aab, et al., Phys. Rev. D93 (12) (2016) 122005.
[49] A. Aab, et al., Phys. Rev. Lett. 116 (24) (2016) 241101.
[50] S. Buitink, et al., Nature 531 (2016) 70.
[51] S. Thoudam, et al., Astronomy & Astrophysics 595 (2016) 33.
[52] W. D. Apel, et al., Phys. Rev. D90 (6) (2014) 062001.
[53] D. Kostunin, et al., Nucl.Instrum.Meth. A742 (2014) 89–94.
[54] C. Glaser, EPJ Web Conf. 135 (2017) 01006.
[55] S. Thoudam, J. R. Hörandel, Astron. Astrophys. 567 (2014) A33.
[56] A. M. Hillas, J. Phys. G31 (2005) R95–R131.